A Novel Laboratory Method for Determining Fine Scale Electrical Resistivity Structure of Core from Contact Measurement of Potential

E.P. Haslam[a *], D.A. Gunn [a], P.D. Jackson [a], Lovell, M.A. [b], Aydin, A. [c], Prance, R.J. [c], and Watson, P [c].

[a]British Geological Survey, Kingsley Dunham Centre, Keyworth, Nottinghamshire, NG12 5GG. ehaslam@bgs.ac.uk. dgu@bgs.ac.uk, Tel: 01159 363327. Fax: 01159 363446 do we have email address for Peter?
[b]Department of Geology, University of Leicester, Leicester, LE1 7RH
mike.lovell@le.ac.uk
[c]Centre for Physical Electronics and Quantum Technology, University of Sussex, Brighton, BN1 9QT

E.P. Haslam[*],
British Geological Survey, Kingsley Dunham Centre, Keyworth, Nottinghamshire, NG12 5GG. ehaslam@bgs.ac.uk. dgu@bgs.ac.uk, Tel: 01159 363327. Fax: 01159 363446

Abstract

The electrical resistivity of water-saturated rocks can be complicated in freshwater-bearing, clay rich formations. Where the pore fluid is saline or the rock is relatively clean, however, the resistivity is known to be a function of both the porosity of the rock and the resistivity and distribution of the pore fluid. We use this established relationship to investigate both sedimentary features and open fractures in rocks through the relationship between electrical resistivity and the distribution of water-saturated-porosity, using novel laboratory instrumentation and procedures. The instrumentation controls multiple contact electrical resistivity measurements made by a single electrode. Core samples are scanned by varying the electrode position in 3-axes over a range of hundreds of millimetres with an accuracy of a tenth of a millimetre. Balance cycle switching of a floating direct current

(DC) source minimises the risk of charge polarisation effects masking the resistivity distribution related to fine scale structure. The single electrode measurements are made with high common mode noise rejection via differential amplification with respect to a reference point within the current flow path. A computer based multifunction data acquisition system logs the current through the sample and voltages along equipotentials from which the resistivity measurements are derived. Multiple measurements are combined to create images of the surface resistivity structure, with variable spatial resolution controlled by the electrode spacing. Although the robot can move in 3-axes, enabling high precision control of the electrode position, the resultant resistivity images are 2D (surface) descriptions. Our results have successfully characterised grainfall lamination and sandflow cross-stratification in a brine saturated, dune bedded core sample representative of a southern North Sea reservoir sandstone, which was studied using the system in constant current, variable voltage mode. In contrast, in a low porosity marble, identification of open fracture porosity against a background very low matrix porosity was achieved using the constant voltage, variable current mode. This new system is limited by the diameter of the electrode which could only practically be reduced to between 0.5 and 0.75 mm. Further work involves trial measurements using a high-impedance, non-contact potential probe in order to reduce the measurement footprint (to the order of 0.1mm) enabling yet higher resolution.

1. Introduction

The electrical resistivity of a porous water-saturated rock depends primarily on the nature of the pore fluid and its quantity and distribution (Archie, 1950). Electrical flow takes place primarily by ionic or electrolytic conduction through the pore fluid, in the absence

of metallic conductors such as pyrite or clay minerals, although the pore fluid properties are affected by salinity, temperature and pressure. In siliciclastic rocks containing significant proportions of clay minerals the presence of a cation-rich layer of electrochemically bound water at the mineral surface can add additional conductivity (Worthington 2011); this effect is due to the negative charge on silicate minerals attracting positive ions and water to the surface, but is small in so-called "clean" sandstones. In "shaly sands", however, with a significant amount of clay minerals this effect can be large due to a large surface area to volume ratio, and can reduce the resistivity (Winsaeur *et al.* 1952; Waxman and Smits, 1968). Here we consider rock formations with relatively small surface conduction effects.

Rock electrical properties are thus sensitive to the mineralogy and the pore morphological characteristics as well as the nature of the pore fluid, degree of saturation, temperature and pressure (Llera *et al*., 1990; Mualem *et al*., 1991, Archie 1942). Most dry rocks are excellent insulators in vacuo, but even saturation with distilled water can decrease resistivity by several orders of magnitude due to the mobilisation of ions for electrical conduction (Duba *et al*., 1978). Archie (1942) published the first quantitative use of electrical resistivity in a petrophysical context and developed a series of empirical yet quantitative relationships linking the resistivity of the water-saturated rock to the pore fluid resistivity through a formation factor previously defined by Sundberg (1932). Archie also related his experimentally-defined formation factor to porosity, and in turn to saturation by incorporating the resistivity of the hydrocarbon bearing rock as well as the resistivity of the water-saturated rock. Today, some 70 years after Archie, these

equations still form the generally accepted basis for the deterministic evaluation of water saturation using electrical methods within petrophysics (Archie, 1950; Burdine *et al*., 1950; Doll *et al*., 1952; Worthington *et al*., 1975; Spandenberg, 2001; Riedel *et al*., 2005, Worthington 2011). Archie's equations rely on the rock matrix being non-conductive and the pore water being relatively saline. Where either of these conditions is contravened, then alternative methods can be employed, based on Archie but with modification to take account of the unusual behaviour (Worthington, 1985; Worthington, 1991; Worthington, 2010) while the combination of shale effects and low salinity may also lead to the electrical resistivity being frequency dependent. In this study we confine ourselves to water-saturated rocks and the relationship between pore fluid distribution as controlled by sedimentary fabric and stress-induced fractures. This understanding forms the basis of electrical resistivity investigations and monitoring at a range of scales, in the laboratory, in the field and in boreholes.

The electrical resistivity distribution is dependent on micro-scale (sub-millimetric) heterogeneity of properties such as porosity, controlled by grain size distribution and cementation, which are strongly related to sedimentological fabrics of millimetric geometries. Thus, small-scale heterogeneity controls the morphology of the pore space and in turn, fluid flow and migration within reservoirs, and this is refelected in the petrophysical properties such as electrical resistivity. Downhole logging tools and techniques have been developed to evaluate and record the heterogeneity within the formation as part of subsurface formation evaluation and conventional downhole logs use current focusing from multi-electrodes, and can identify bedding and fractures with

vertical resolutions of 200 mm (Schlumberger, 1993), whereas, downhole electrical imaging devices comprising multi-electrode-button pads on several pads contained on radial arms provide images with approximately 5 mm resolutions (Schlumberger, 2004; Weatherford, 2006). Images provided by the high resolution downhole tools, however, require quantitative calibration and while possible by integrating the borehole images with resistivity measurements made downhole using conventional resistivity logs, the latter often have a poor resolution and calibration can be problematical (e.g. Ekstrom *et al*., 1986; Boyeldieu & Jeffreys, 1988). Calibration may be feasible using laboratory measurements on core samples taken from the borehole. Thus, assessing the resistivity of core at the millimetre scale achieved in downhole image logs would be beneficial (Lovell *et al*., 1997; Lovell *et al*., 2006).

This paper concerns the development of laboratory techniques that are capable of making resistivity measurements with the required resolutions to capture the fine sedimentological fabric within reservoir rocks. Both galvanic or contacting and non-contacting techniques for high-resolution rock core resistivity measurements have been previously developed. By measuring the voltage gradient parallel to a switched DC current across fixed, multi-electrode grids Jackson *et al* (1991, 1992, 1995) produced resistivity images with a 5 mm resolution of the fabric in samples of the Penrith Sandstone. These images were used within a study of the control of fine scale dune bedded structures on the flow of fluids through aeolian sandstone analogues to the Rotliegendes Formation of the Southern North Sea (Lovell *et al*., 1995; Harvey *et al*., 1995; Lovell *et al*., 2006). Using a primary and secondary coil pair, Jackson *et al* (1997,

2006) also developed an electromagnetic, non-contacting technique based upon measurements of the secondary magnetic field induced by current flow within brine-saturated sandstone. These measurements were made at low induction numbers where the skin depth was far greater than the coil separation and the strength of the secondary magnetic field was controlled by the rock conductivity (reciprocal of resistivity). The coil separation of 40 mm enabled the method to be sensitive to resistivity changes over 15 mm axial resolution. Improving the resolution of the non-contact method would require re-engineering of small coils with closer separations, which would require miniaturisation techniques. Increasing the resolution of the contact method, however, only requires a means of reducing the spacing within the electrode grid. The main system described here in this paper achieves this by replacing a fixed grid of electrodes with a single robotically controlled electrode capable of very fine movements of as little as 100 microns; the increased scanning time required to move a single electrode is not considered to be a serious disadvantage. A key technical aspect of this paper, however, is the design of measures to overcome potential charge polarisation obscuring the fine detail in the resistivity image and also, to minimise spurious potentials associated with buffering the voltage measurements made with repeated contact of the single electrode. We also show how the system can be applied to optimise the resistivity imaging of fine scale, millimetric features determined by sedimentological fabric and fractures.

In addition to these developments, we have also experimented in inferring the electrical resistivity of a sandstone formation using a new sensor technology, the Electric Potential

Sensor (EPS or EP Sensor), invented and patented by the University of Sussex (Prance *et al.*, 2000). The EPS is a generic sensor technology, which can be configured to measure electric field, static charge or spatial potential, in a non-invasive, non-contact manner. Its use has been demonstrated in many areas of application, and include non-contact imaging of carbon composite structures (Gebrial *et al*., 2006, 2007), and the detection of electric field in rock, induced by uniaxial compression (Aydin *et al*. 2009). This latter application to rocks is an example of the detection of signals generated from within the rock. To infer the resistivity an AC current is used to generate a spatial potential above the specimen that varies with the local resistivity of the rock structure. Using a suitability fine electrode, the ultra-high input impedance of the EP Sensor allows for the imaging of the surface potential through a raster scan. A preliminary scan of a sandstone sample is presented which offers complementary findings to that of the galvanic method. A single line scan between the electrodes applying the current through the sample also confirms Ohm's law.

2. Measurement Principles

The development of electrical resistivity imaging of cores using four-electrode contact measurement technology is well documented (Jackson *et al*., 1990; Lovell & Jackson, 1991; Jackson *et al*., 1991; Jackson *et al*., 1992; Lovell *et al*., 1994; Harvey *et al*., 1994; Jackson *et al*., 1995; Lovell *et al*., 1997). The technique was developed to produce quantitative resistivity data on core at a similar resolution to that of a downhole imaging device. The core images may be used to quantitatively constrain the fine scale structural changes seen on downhole images and provide a means of defining the variability of the electrical resistivity structure of a formation. Furthermore, these core images have the potential to provide an interpretation of downhole images in terms of fine-scale

petrophysical structures. Practical implementation of the four-electrode method required independent measurement on two voltage electrodes of the potential field caused by distributed current flowing through the sample (see Fig. 1). Resistivity is determined by multiplying a resistance based upon a straightforward voltage-current ratio with a geometric factor that is related to the current distribution within the sample. High-resolution images of rock structures are created by using a sample-electrode arrangement whereby a constant current of uniform density flowed in a direction that was normal to the planar structures within the sample. Therefore, any series of collinear voltage measurements made perpendicular to the uniform current flow will be on equi-potential lines that are co-planar with the sample structure, (Figure 1a). Resistivity variation, and thus sedimentological structure, can be imaged via the localised potential gradient. Techniques to increase the region of uniform current flow include use of multiple, balanced electrodes (Jackson *et al*., 1995) in conjunction with small, saturating fluid reservoirs extending beyond the length of the sample (Figure 1b). Formerly, the voltage measurements were made via individually scanning electrodes within a permanent, fixed grid. This approach limited spatial resolution to the grid spacing and total lateral grid coverage to the channel limitations of the scanning multiplexer. The settling time required after each individual electrode was switched to the impedance buffering circuits also affects voltage measurement time and accuracy. Jackson *et al* (2002) overcame these problems by hardwiring every voltage electrode to its own impedance buffer and digitally multiplexing the buffered outputs onto a common 16-bit bus. While vastly increasing accuracy and switching speeds, this approach requires additional instrumentation and has limited flexibility in relation to grid size / resolution adjustments. This system is applied

as the concept for a laboratory based, single channel, moveable electrode, fine scale contact resistivity imager below.

Figure 1. Current spreading at electrodes and distribution within a sample for different electrode arrangements.

2.1 Instrumentation and Method

A system has been developed that can pass a uniformly distributed direct current through each sample without developing charge polarisation due to net ionic migration. This is achieved by balanced switching of a DC constant current source (0.5 – 50mA range) such that equal cycles of current flow alternate in opposite directions along the sample (Figure 1a and 1b) such that any net charge accumulation, AC effects and any effects associated with the reapplication of the moving electrode are eliminated. The complete system (Figure 2) comprises the following modules: (1) Timer, which controls the current switching and measurement cycles; (2) Floating Constant Current Source, which provides a constant current regardless of load impedance, signal conditioning module, including (3) Differential Amplification buffers for the current and voltage measurements; (4) Sample & Hold to capture the peak DC levels; and (5) Filter/Amplification of signals that are acquired by (6) PCMCIA PC Data Acquisition Control (DAQ) card, which also manages the movement of (7) the Three-axis Robot that carries the voltage electrode, P1. The overall operational procedure involves current being driven into the saline reservoirs at either end of the sample holder via electrodes C1 and C2, and through the saturated rock core sample, generating potentials that are measured at points along the rock surface via electrodes P1 and P2. Essentially, this forms the basis of a 4-point measurement system; one of the electrodes, however, provides a fixed reference point while the other is

controlled by a robot and can move freely around the sample. This approach enables voltage measurements to be made across the surface of the sample. Previous systems have utilised fixed voltage electrode arrays where array separation, to accommodate variable resolution of measurement, is not readily achieved. The robot is controlled in such a way that the moving phosphor bronze electrode is lifted and placed onto the surface of the sample where it is allowed to (electrically) settle before a measurement is made. It is then moved to the next position and the process is repeated. In this way, a voltage potential map, or resistance per pixel, can be determined. By measuring many points, and taking the differential of the successive measurements, a two dimensional resistivity map of the core sample surface can be obtained. Grid coordinates are pre-programmed into the computer and located with a potential resolution of +/- 100 microns. The electrode array described above (i.e. pole-pole) also has the advantage of a high signal-to-noise (S/N) ratio. The system is capable of acquiring a two-point measurement using two electrodes; a moving electrode, however, offers flexibility and higher single point resolution to image structures in low resistivity rocks with very high primary porosity, such as a dune-bedded sandstone. The same is also true in highly resistive rocks where open fractures contribute to the secondary porosity against a low matric porosity. In either case, resistivity images aid interpretation of pore space connectivity, and, in turn, qualitative permeability and flow patterns, by identifying sedimentological fabric as delineated by changes in porosity, or by distinguishing between open or closed (i.e. cemented) fractures. Electrode-probe designs can be adapted to match the requirements of the measurement; for example a solid 1 mm diameter phosphor bronze tip enables high resolution measurements with very low

voltage offsets on low resistivity rocks, while a fibre-tipped probe maintains an ionic pathway when imaging conductive fractures in very high resistivity rocks.

Figure 2. System schematic of the core imaging instrumentation.

A Visual Basic programme controls the interface logic that acknowledges the robot is in position for a measurement, switches on the power to the floating current source module, acquires the measured voltages and other parameters, and sends a logic pulse to move the robot to the next measurement position.

3. Results

3.1 Calibration Tests

Four machines were tested in order to reveal the accuracy contour of the measured resistance versus the drive current (Table 1). Test resistance loads were chosen to a tolerance of 0.5%. In order to average out any interference effects from the mains AC supply, tests were undertaken with the current switching frequency below 50 Hz (UK mains). A four point measurement was carried out across the load at a constant temperature. The results shown in black indicate the optimised operational load-current range of the instrument, i.e. of the order of 0.1V – 20V over the test load. Results shown (Table 1) in blue indicate that the voltage across the load has reached 20V, which represents the maximum potential difference available and results in a limiting of the current flowing through the test load. The readings in red indicate where the instrument is either under or over-voltage, which leads to poor reading accuracy. When this situation is encountered, a warning message is displayed on the LCD display.

3.2 Constant Current – Imaging Sedimentary Structure

The set-up in figure 1 was used for measurements on low resistivity rocks, typically of the order of kilo ohms, where the sample can be considered as a distributed network of resistors and the resistance between more porous bands is lower than the resistance throughout less porous bands. In this set-up, a constant current flows through the total resistance of the network and thus, by taking the gradient of the voltage measurements along the y-axis, an image of the structure of the core can be generated. Single potential measurements were taken over the core sample and the differences between neighbouring measurement points along the y-axis were plotted. A gradient was not calculated with respect to the x-axis as this was aligned parallel to the structural lamination. Contact resistances were measured and found to be small and of the order of < 2 kΩ, and therefore no additional measures were required to correct for these. Steps could have been taken to reduce this; such as using a higher conductivity saturating fluid. The sample was wetted throughout the tests and never allowed to dry out, as this could affect the pore water properties and the surface conductivity. The Experiment was maintained at a constant temperature of 20^{o}C. During the tests, the y-incremental electrode spacing was varied from 6 mm to 0.5 mm and the current was varied from 10 – 30 mA in order to find optimum minimum and maximum operating parameters. In the studies here it is assumed that there is a constant resistivity structure throughout the height of the rock, and to this end the rock is prepared so the current flow is orthogonal to the sedimentological structure (and the x-axis). Image resolution can be improved through increasing the spatial resolution by reducing the y-incremental electrode spacing. Best results were found when reducing the y-incremental electrode spacing was accompanied by an increase in the current, which is considered to be related to increasing the amplitude of

the voltage difference measurements above the system noise floor. Figure 3 shows the improved resolution gained by reducing the y-incremental spacing from 4 mm to 1 mm combined with an increase in current from 12 mA to 30 mA, where structure within fine laminations appears only at the highest resolution. The photograph of the sample surface is also presented for comparison.

Figure 3. Structural detail within electrical images of a dune-bedded sandstone: a. Photo of rock surface; b. Δy=4 mm / I=12 mA; c. Δy=1 mm / I=30 mA .

This sandstone comprises 85% quartz grains with minor lithic fragments (gneiss), feldspar, mica and opaques. The grain size range has an overall bimodal distribution, predominately falling within 25 to 250 μm or 0.5 to 1 mm. Higher voltage gradients in the upper half of the sample are generally associated with the smaller grain size distributions ranging from coarse silt to fine sand in a relatively densely packed structure. In contrast, the lower half of the sample has a denser fabric inter-laminated with more loosely packed bands of well-rounded coarse sand. A conductive saturating fluid was required in order to reduce contact resistances. Typical resistivity of the saturating fluid was measured to be 0.25 Ω.m and the scale bar is graduated as a multiple factor, which in this case equates to resistivities from 10 Ω.m to 30 Ω.m. Increasing current flow to 30 mA, appeared to improve signal to noise ratios by increasing the measured voltages over the core surface. Again, this improvement can be seen in better delineation of the fabric within the image. Note how the banding in the lower section is better resolved and also how more distinct banding in the central section is developing the resistivity of bands of more loosely packed, thinner laminations. By combining the benefits of increased signal to noise ratio and improved spatial resolution, it can be observed that a far more complex

structure to the lower, banded section of the core sample emerges (Figure 4). These images have been interpreted as showing grainfall lamination and sandflow cross stratification found in dune-bedded Permo-Triassic sandstones within the Eden Valley and Carlisle Basins of the UK (Reading, 1981; Walker *et al*., 1984; Benton *et al*., 2002). The grainfall laminae result from wind transportation and deposition from suspension of well-sorted, well-rounded millimetre-sized grains in a high porosity, loose packing. The sandflow laminae result from minor slippages along the leeside of the dune along laminations of coarse silt, producing a denser packing with a more poorly-sorted grain size range from silt to sand classes (Harvey *et al*., 1995).

Figure 4. *Constant current measurements, with 20 mA of injected current, 1mm x-axis and 0.5 mm y-axis resolution.*

3.3 Constant Voltage – Fracture Mapping

In this mode, superior results were obtained by introducing the current at the contact point between a fibre tipped voltage measuring probe and the rock surface via ionic flow within fluid absorbed in the porous fibres. Voltage measurements were made between the base of the fibre from an electrode positioned just above the core sample surface and the reference point C2 (Figure 2). Total current flow was monitored via a voltage measurement across a standard resistor network (between I1 and C2) that is in series with the load provided by the core sample. Current flow in this set-up would be limited mainly because of the highly resistive rock, typically of the order greater than tens of kilo-ohms, as the voltage is kept constant. A variable current style of measurement would therefore be made. Figure 5 shows the result of constant voltage, variable current

measurements carried out on a highly resistive, fractured rock sample using the constant current probe configuration described above. Note from the image of the core surface that the more conductive area is following the path of the fracture and other smaller, interconnected fractures. The remainder of the core surface is less conductive and hence more resistive, limiting the current flow. The fracture generally appears less resistive, and at the measurement level, a lower resistive path through the core would have caused greater overall current flow through the network such that a constant voltage would have been maintained. The constant voltage method therefore appears to be ideal for fault or fracture detection and analysis where fractures are either open and fluid filed, or closed and cemented with a non-conducting mineral such as quartz or calcite. In this case, the lower resistance of the fracture is an indication that it is open and fluid filled, rather than a closed, cemented fracture. The surfaces of very low permeability rocks can be analysed with this system to assess the proportion of open to closed fractures on the basis of thresholds within the conductance or resistivity images, although the presence of clay-filled fractures may give similar responses to open fractures depending on the nature of the clays and the conductivity of the pore fluid. It may be feasible to develop a series of indices relating to the fracture flow potential within the rock on the basis of these analyses.

Figure 5. Constant voltage measurement set-up and image on high resistivity, fractured core sample.

3.4 Electric Potential Sensor surface and line scans

A new sensor technology, the Electric Potential Sensor (EPS or EP Sensor can be configured to measure electric field, static charge or spatial potential, in a non-invasive, non-contact manner. To infer the resistivity an AC current is used to generate a spatial potential above the specimen that varies with the local resistivity of the rock structure. A preliminary electric potential scan of a sandstone specimen surface potential is presented in Figure 6. A 0.2 mm electrode probe was used to scan a central area of 25.2 mm x 25.2 mm. The probe is not in contact with the formation but is in very close proximity, smaller than the electrode diameter. The step increment size is 126 μm, scanned in a raster fashion. The two images depict (a) the EPS output voltage map and (b) the EPS output phase map for the same raster scan. The two images offer different contrasts of identical features on the sample spatial surface potential.

Figure 6. EPS surface scan of sandstone specimen; (a) voltage output data, (b) output phase data.

Figure 7 shows the results for a line scan of the sandstone sample through its central axis from the input to the grounded electrodes. The data for the EPS output amplitude and phase over the single line are shown. The amplitude has a clear Ohm's law slope and the fluctuations around this quantify the local conductivity variations.

Figure 7. EPS line scan through length of sandstone specimen. Results show the EPS output voltage and phase.

4. Discussion

Micro-scale features such as grain size distribution and porosity distribution, control fluid migration and flow, as well as the trapping of oil and gas within reservoirs. This is because the capillary pressure and wettability are important processes in fluid behaviour in porous materials and these are significantly dependent on the pore size. Borehole imaging tools can identify these features within a formation as part of reservoir evaluation. The downhole images require quantitative calibration and a resistivity imaging method has been developed that can be used as part of core-borehole log integration procedures to enhance the study of the fine scale sedimentological features in water-saturated porous, permeable formations, even at low porosities.

The system can be configured to operate in two modes for the rapid, high-resolution analysis of both high-resistivity fractured rock and low-resistivity highly porous core samples. The sedimentological features in a brine-saturated rock with high primary porosity can be studied using the system in constant current, variable voltage mode. Fracture porosity can be studied in very low porosity rocks using the constant voltage, variable current mode. Experimental results on dune-bedded Penrith sandstone core demonstrate the effectiveness of the first approach, while results for a marble core sample show the applicability of the latter in the analysis of fractured core.

This novel measurement produces fine scale images of the samples with millimetric resolution, for example identifying the fabric associated with bimodal grainsize-porosity distributions resulting from scour, granule lags and cross-lamination caused by wind driven dune deposition and slumping in a desert environment (Figure 3). These resistivity images enable high-resolution evaluation of the rock porosity within a porous,

permeable reservoir and reveal fine scale detail of fining up sequences. Features such as these are often associated with the deposition processes whereby wind-blown, Aeolian deposits of varying grain size have been deposited sequentially. Coarser deposition bands relate to greater porosity and therefore lower resistivity while finer bands, often with greater quartz cementation, have a lower porosity and a greater resistivity (Lovell *et al*., 2006). As Figure 4 illustrates, there has been some success in imaging these fabrics, with Δy resolutions as low as 0.5 mm being used in order to achieve these results. The disadvantage of the system, however, is the physical limit imposed by the phosphor bronze electrode, which equates to approximately 0.5 mm. Further improvements on resolution could be made by reducing, in turn, the physical size of the probe tip and the Δy resolution, or the development of a non-contact probe that would totally eliminate issues such as contact resistance.

The existing system may be further improved, for example, with the elimination of high voltages presented to the instrumentation amplifier input stage whilst injecting current into highly resistive rocks. Currently, the divider network at this point reduces the common mode rejection ratio via the imbalance of the low tolerance network resistors and also introduces input offset voltages caused by the input bias current of the instrumentation amplifier. These input offsets are further amplified down the chain. It also has the effect of reducing smaller signals to the point at which they could be masked by noise, hence the need to apply higher injection currents in our experiments. At present however, the input offsets were measured and found to be larger than the noise floor of the system, but it is possible to calibrate this effects out of the system. Detection and automatic adjustment of the input signal and conditioning it to a suitable level, prior to

the instrumentation amplifier, is a possible improvement, using the raw signal without reducing the quality of the signal prior to amplification. At present the system is capable of sourcing 0.5 – 50mA of current at 20V. This yields a sample test range of approximately 400 Ω to 40 kΩ. Further improvements have been made to the current source to allow lower currents (typically 50 μA) to be injected and allow further testing of existing samples at lower currents and to allow higher resistivity samples to be investigated.

The preliminary electric potential measurements using the EP Sensors clearly provide an additional non-contact advance on scanning the sandstone, which evidently follows expected Ohmic laws. Future work using this approach may offer a more rapid, higher resolution resistivity scanning of that achievable using non-galvanic approaches. It would also negate the need for an electrode to contact the sample i.e. non-galvanic coupling. Further work is needed to explore this approach and seek to calibrate and comprehensively compare it with the galvanic contact technique. The added benefit of having a non-contact system is that the sample may be imaged through its plastic core liner and remain uncontaminated. The challenges to this approach include overcoming the loss of signal strength that occurs as the area of the electric potential sensor is reduced and as the offset distance between the sensor and the rock surface is increased. But if these challenges are overcome, the EP Sensor offers the potential for sub-millimetric image resolution and better imaging of fine scale detail of fining up sequences.

Wider application of this core imaging approach to hydrocarbon reservoirs has yet to be demonstrated, but where conductive paths exist in the rock it may yield useful additional core imaging on which to base further research and special core analysis, even in shale

gas and shale oil plays if the formation water is highly conducting and the rock has a non-zero effective porosity, such as in the Haynesville and Marcellus.

Conclusions

1. We have successfully developed and demonstrated novel electrical resistivity measurements for use on water-saturated core with high spatial and measurement resolution.
2. Current is injected into the core sample and the electric field measured by rapidly scanning the probe at very fine increments along the core surface. By increasing the resolution of the scanned probe over a fixed grid, and improving the signal to noise ratio, it is possible to build up a resistivity map that is fine enough to resolve sedimentological features.
3. Four-electrode measurements effectively allow electrical resistivity images to be acquired that result from resistivity variations associated with sedimentological fabrics associated with deposition and diagenesis processes in the form of primary and secondary porosity.
4. Image fidelity is improved via balanced, floating DC current source switching that minimises charge polarisation effects masking fine-scale structure.
5. Using constant current flow a range of fabrics resulting from depositional and diagenetic processes can be identified in a fully brine-saturated dune bedded sandstone.
6. When operated in variable current mode, the system can image relatively high resistivity, fractured rocks to differentiate conducting fractures from non-conducting fractures (as higher current flow, lower relative resistivity features).

7. Movement increment and repeatability and electrode diameter impose limitations on the system capability, both of which could be improved via improved precision engineering. Other limitations include settling times of the measuring amplifiers associated with galvanic voltage measurements.
8. These limitations can be overcome and imaging time significantly reduced by using non-galvanic (non-contact) methods of electric field measurement that draw virtually zero current. These methods have been shown in brief, but require further investigation.

Acknowledgements

The contributions of E. P. Haslam, D. A. Gunn and P. D. Jackson are published with the permission of the Executive Director of the British Geological Survey, NERC.

References

Archie, G.E., 1942; *The electrical resistivity log as an aid in determining some reservoir characteristics.* Petroleum Transactions of AIME, 146, 54-62.

Archie, G.E., 1950; *Introduction to geophysics of reservoir rocks*. Bull. AAPG 34, 943-961.

Archie, G.E. (1950). "Introduction to petrophysics of reservoir rocks". *American Association of Petroleum Geologists Bulletin* **34** (5): 943–961.

Aydin, A., R. J. Prance, H. Prance, and C.J. Harland, 2009; *Observation of pressure stimulated voltages in rocks using an electric potential sensor*. Applied Physics Letters, 95, 124102.

Benton, M., E. Cook, and P. Turner, *Permian and Triassic Red Beds and the Penarth Group of 2002*; Great Britain, Geological Conservation Review Series, Joint Nature Conservation Committee, Peterborough, No. 24, 337p.

Berg, C. R., 2007; *An effective medium algorithm for calculating water saturations at any salinity or frequency*. Geophysics, 72, E59-E67.

Boyeldieu, C., and P. Jeffreys, 1988; *Formation microscanner: new developments*. In: 11th European Formation Evaluation Symposium Transactions. Society of Professional Well Log Analysts, paper WW.

Burdine, N. T., L. S. Gournay, and P. P. Reichertz, 1950; *Pore size distribution of petroleum reservoir rocks*. Petroleum Transactions of AIME, 189, 195-204.

Clennell, B.M 1997. Tortuosity: a guide through the maze. Geological Society of London, Special Publication. 122. doi: 10.1144

Doll, H. G., R. Sauvage, and M. Martin, *Application of micro logging to determination of porosity*. Oil & Gas Journal. 1952; 51, (18), 86-94.

Duba, A., A. J. Piwinskii, M. Santor, and H. C. Weed, 1978; *The Electrical Conductivity of Sandstone, Limestone and Granite*, Geophysics. Journal of Royal Astronomical Society, 53, 583–597.

Ekstrom, M., C. A. Dahan, M. Chen, P. M. Lloyd, and D. J. Rossi, 1986; *Formation imaging with microelectrical scanning arrays*. In: 27th Annual Logging Symposium Transactions. Society of Professional Well Log Analysts, paper BB.

Gebrial, W., R. J. Prance, C. J. Harland, P. B. Stiffell, H. Prance, and T. D. Clark, 2006; *Non-contact imaging of carbon composite structures using electric potential sensors*. Measurement Science & Technology, 17(6), 1470-1476.

Gebrial, W., R. J. Prance, R. J. Harland, P. B. Stiffell, H. Prance, and T. D. Clark, 2006; *Non-contact imaging of carbon composite structures using electric potential sensors*. Measurement Science & Technology, 17(6), 1470-1476.

Gebrial, W., R. J. Prance, C. J. Harland. T. D. Clark, 2007; *Non-invasive imaging using an array of electric potential sensors*, Review of Scientific Instruments, 77(6), DOI: 10.1063/1.2213219.

Harvey, P. K., P. D. Jackson, M. A. Lovell, G. Williamson, J. K. Ball, A. P. Ashu, A. S. Smith, and R. C. Flint,1994; *Structural implications from fluid flow and electrical resistivity images in aeolian sandstones*. SPWLA 35th Annual Logging Symposium, Paper LL, p.1-7.

Harvey, P. K., M. A. Lovell, P. D. Jackson, A. P. Ashu, G. Williamson, A. S. Smith, J. K. Ball, and R. C. Flint, 1995; Electrical core imaging III: Characterisation of an Aeolian Sandstone. Scientific Drilling, 5, 164-176.

Jackson, P. D., M. A. Lovell, C. A. Pitcher, C. A. Green, C. J. Evans, R. C. Flint, and A. Forster, 1990; Electrical resistivity imaging of core samples. Transactions of the European Core Analysis Symposium (EUROCAS I).

Jackson, P. D., and ODP Leg 133 Shipboard Party. 1991; *Electrical resistivity core scanning: a new aid to the evaluation of fine scale sedimentary structure in sedimentary cores*. Scientific Drilling, v.2, 41-54.

Jackson, P. D, M.A. Lovell, P. K. Harvey, J. K. Ball, C. Williams, A. P. Ashu, R. C. Flint, P. I Meldrum, G. Reece, and G. Zheng, 1992; *Electrical resistivity core imaging: - theoretical and practical experiments as an aid to reservoir characterisation*. Society of

Professional Well Log Analysts (SPWLA), 33rd Annual Logging Symposium, Paper VV, p.1-13.

Jackson, P. D., M. A Lovell, P. K. Harvey, J. K. Ball, P. Williams, R. C. Flint, D. A. Gunn, A. P. Ashu, and P. I. Meldrum, 1995; *Electrical resistivity core imaging 1: a new technology for high resolution investigation of petrophysical properties*. Scientific Drilling, 6, 4, 139-152.

Jackson, P. D., D. A. Gunn, R. C. Flint, D. Beamish, P. I. Meldrum, M. A. Lovell, P. K. Harvey, and A. Peyton, 1997; *A non-contacting resistivity imaging methods for characterising whole round core while in its liner*. In Lovell, M.A. & Harvey, P.K. (Eds.), Developments in Petrophysics. Geological Society of London Special Publication, No. 122, 1- 10.

Jackson, P. D., R. C. Flint, K. Briggs, R. Holyer, and J. Sandidge. 2002; *Two- and three-dimensional heterogeneity in carbonate sediments using resistivity imaging*. Marine Geology, 182: 55-76.

Jackson, P. D., M. A. Lovell, J. A. Roberts, P. J. Schultheiss, D. A. Gunn, R. C. Flint, A. Wood, R. Holmes, and T. Frederichs. 2006; *Rapid non-contacting resistivity logging of core*. In. Rothwell, R.G. (Ed.), New techniques in sediment core analysis. Geological Society of London Special Publication, SP 267.

Llera, F. J., M. Sato, K. Nakatsuka and H. Yokoyama, 1990; *Temperature Dependence of the Electrical Resistivity of Water-Saturated Rocks.* Geophysics, 55, 576–585.

Lovell, M. A. and P. D. Jackson 1991; *Electrical flow in rocks: the application of high resolution electrical resistivity core measurements*, paper WW in 32nd Annual Logging Symposium Transactions: Society of Professional Well Log Analysts (SPWLA).

Lovell, M. A., P. K. Harvey, P. D. Jackson, J. K. Ball, A. P. Ashu, R. C. Flint, and D. A. Gunn, 1994; *Electrical resistivity core imaging: towards a 3-dimensional solution*. Society of Professional Well Log Analysts (SPWLA), 35th Annual Logging Symposium, Paper JJ, p.1-6.

Lovell, M. A., P. K. Harvey, P. D. Jackson, R. C. Flint, D. A. Gunn, G. Williamson, J. K. Ball, A. P . Ashu, and C. Williams, 1995; *Electrical core imaging II: investigation of fabric and fluid flow characteristics*. Scientific Drilling, 5, 153-164.

Lovell, M. A., P. K. Harvey, C. G. Williams, P. D. Jackson, R. C. Flint, and D. A. Gunn, 1997; *Electrical Resistivity Core Imaging: a petrophysical link to borehole images*. The Log Analyst 38, 6, 45-53.

Lovell, M. A., P. D. Jackson, P. K. Harvey, and R. C. Flint, 2006; *High-resolution petrophysical characterization of samples from an aeolian sandstone: the Permian Penrith sandstone of NW England*. In: Tellam, J. H., and R. D. Barker. (eds). Fluid Flow and Solute Movement in Sandstones: The Onshore UK Permo-Triassic Red Bed Sequence. Geological Society of London Special Publication, 263, 49–63.

Mualem, Y., and S. P. Friedman, 1991; *Theoretical prediction of electrical conductivity in saturated and unsaturated soil*. Water Resources Research. 27, (10), 2771-2777.

Prance, R. J., A. Debray, T. D. Clark, H. Prance, M. Nock, C. J. Harland, and A. J. Clippingdale, 2000; *An ultra low noise electric potential probe for human body scanning*. Measurement Science & Technology, 11, 291-297.

Reading, H. G., 1981; *Sedimentary environments and facies*. Blackwell Scientific Publications, Oxford, 569p.

Riedel, M., Collett, T.S. & Hyndman, R.D. 2005; *Gas hydrate concentration estimates from chlorinity, electrical resistivity and seismic velocity*. Geological Survey Canada. Open-File Report, 4934.

Spandenberg, E., 2001; *Modelling the influence of gas hydrate content on electrical properties of porous sediments*. Journal of Geophysics Research, 106 (B4), 6535-6548.

Sundberg, K. 1932. Effect of impregnating waters on electrical conductivity of soils and rocks. Society of Mining and Engineering Transactions, volume 97. Reprinted by Society of Professional Well Log Analysts, 1980, The Log Analyst, volume 21 (3), 32pp.

Walker, R. G., *Facies Models.* 1984; Geoscience Canada Reprint Series 1. Geological Society Canada Publications. 317p.

Waxman, M.H.; Smits, L.J.M. (1968). "Electrical conductivities in oil-bearing shaly sands". *SPE Journal* **8** (2): 107–122. doi:10.2118/1863-A

Weatherford., 2006; *High resolution microimager (HMI) tool*. 2p.

Winsauer, W.O.; Shearing, H.M., Jr., Masson, P.H., and Williams, M. (1952). "Resistivity of brine saturated sands in relation to pore geometry". *AAPG Bulletin* **36** (2): 253–277.

Worthington, G.F. and D. H. Griffiths, 1975; *The application of geophysical methods in the exploration and development of sandstone aquifers*. Quarterly Journal of Engineering Geology, 8, 73-102.

Worthington, P. F. , 1985. The evolution of shaly-sand concepts in reservoir evaluation. The Log Analyst , 26; 1, P 23-40

Worthington, P.F. 1991. Quantitative evaluation of hydrocarbon saturation in shaly freshwater reservoirs. The Log Analyst, July-August. pp358-370

Worthington, P.F., 2010.Quality assured evaluation of freshwater-bearing hydrocarbon reservoirs. Society of Petroleum Engineers, 133898, 11pp.

Worthington, P F. 2011. Petrophysics of Problematical Reservoirs. Journal of Petroleum Technology. pp 88-97.

Figure Captions (note colour figures 6, 7 & 8 below)

Figure 1. Current spreading at electrodes and distribution within a sample for different electrode arrangements

(after Jackson *et al*. 1991).

a. Fundamental four-electrode resistivity measurement.

b. Multiple current electrodes to extend uniform current flow within sample.

Figure 2. Schematic representation of the core imaging system

Figure 3. *(Colour)* Sedimentological fabric detail within electrical images of a dune-bedded sandstone. The variation in resistance is due to the contrast in resistivity between more porous bands (lower) than and less porous bands (higher):

a. Photo of rock surface;

b. Dy 4 mm / I 12 mA;

c. Dy 1 mm / I 30 mA

Figure 4. *(Colour)* Constant current measurements, with 20mA of injected current, 1mm x-axis and 0.5mm y-axis resolution.

Figure. 5 *(Colour)* Constant voltage measurement set-up and image on high resistivity, fractured core sample.

Figure 6. EPS surface scan of sandstone specimen; (a) output voltage data, (b) output phase data.

Figure 7. EPS line scan through length of sandstone specimen. Results show the EPS output voltage and phase.

Figures

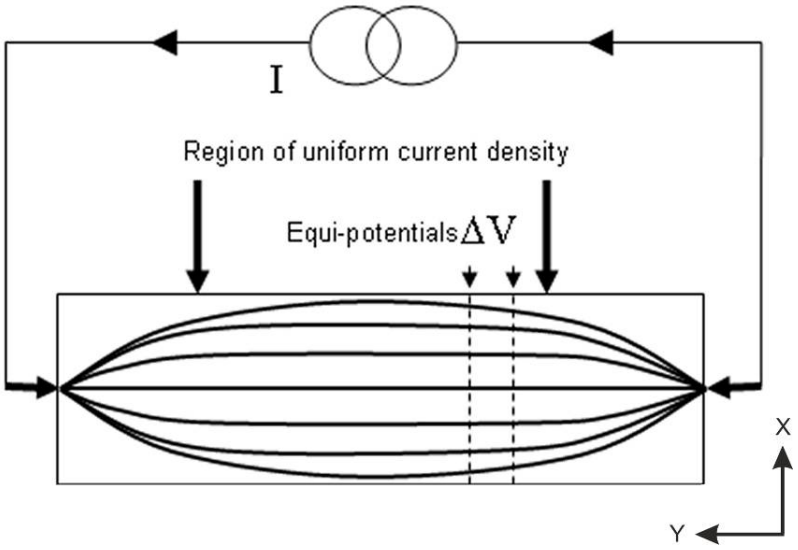

Figure 1a. Current spreading at electrodes and distribution within a sample for different electrode arrangements.

Figure 1b. Current distribution within a sample for different electrode arrangements.

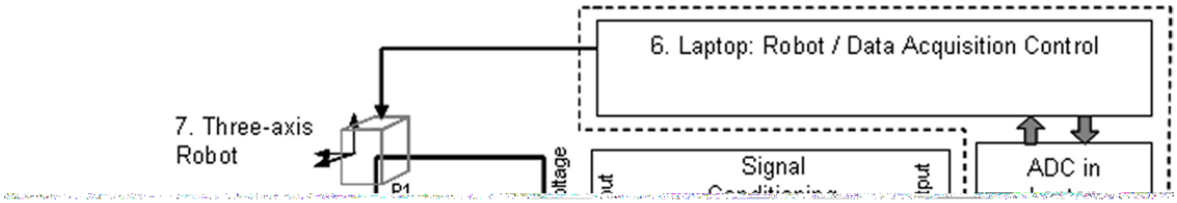

Figure 2. System schematic of the core imaging instrumentation.

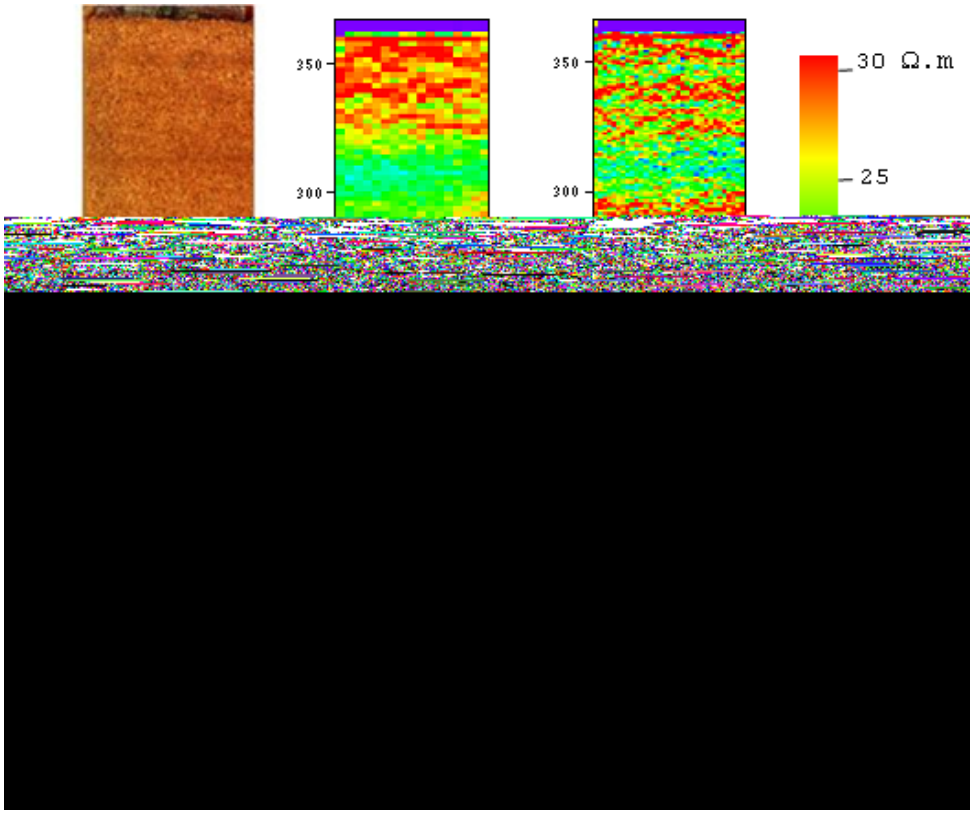

Figure 3. Sedimentological fabric detail within electrical images of a dune-bedded sandstone. The variation in resistance is due to the contrast in resistivity between more porous bands (lower) than and less porous bands (higher): a. Photo of rock surface; b. Δy=4 mm / I=12 mA; c. Δy=1 mm / I=30 mA .

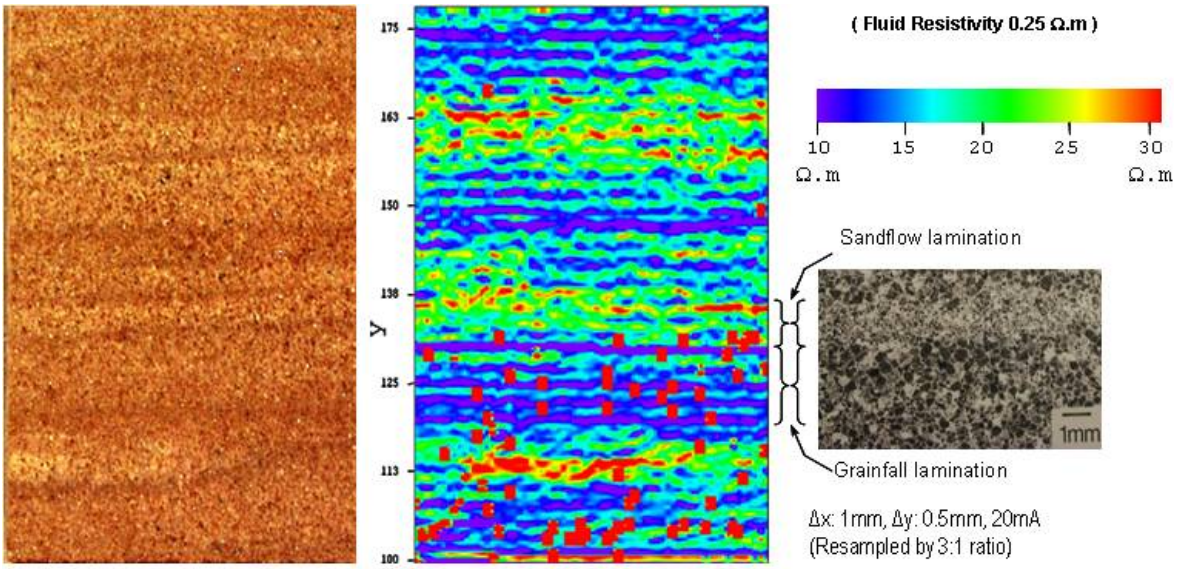

Figure 4. Constant current measurements, with 20 mA of injected current, 1mm x-axis and 0.5 mm y-axis resolution.

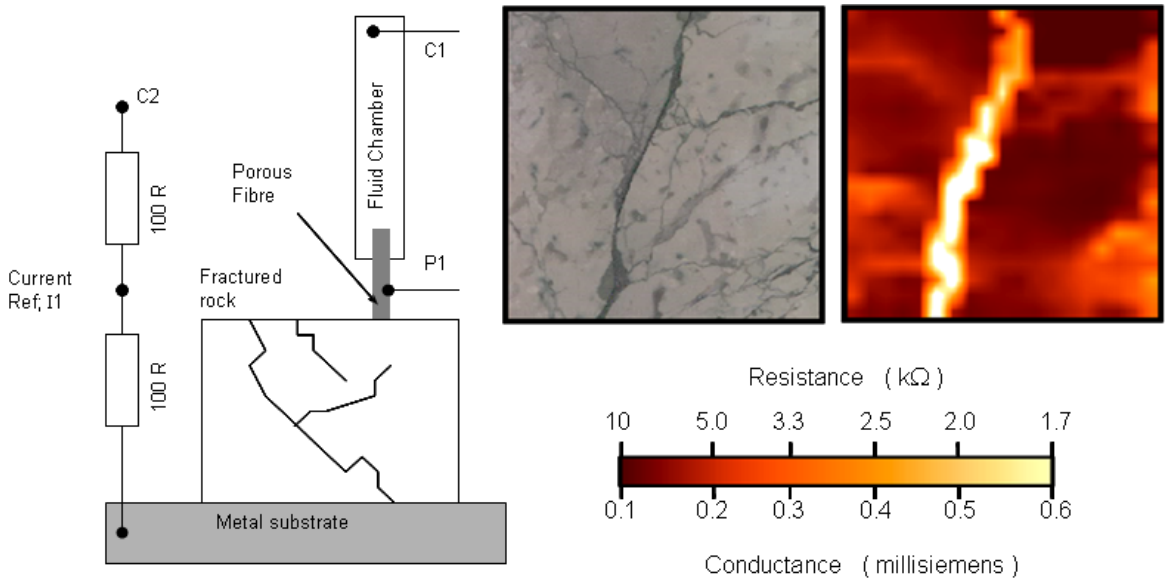

Figure 5. Constant voltage measurement set-up and image on high resistivity, fractured core sample.

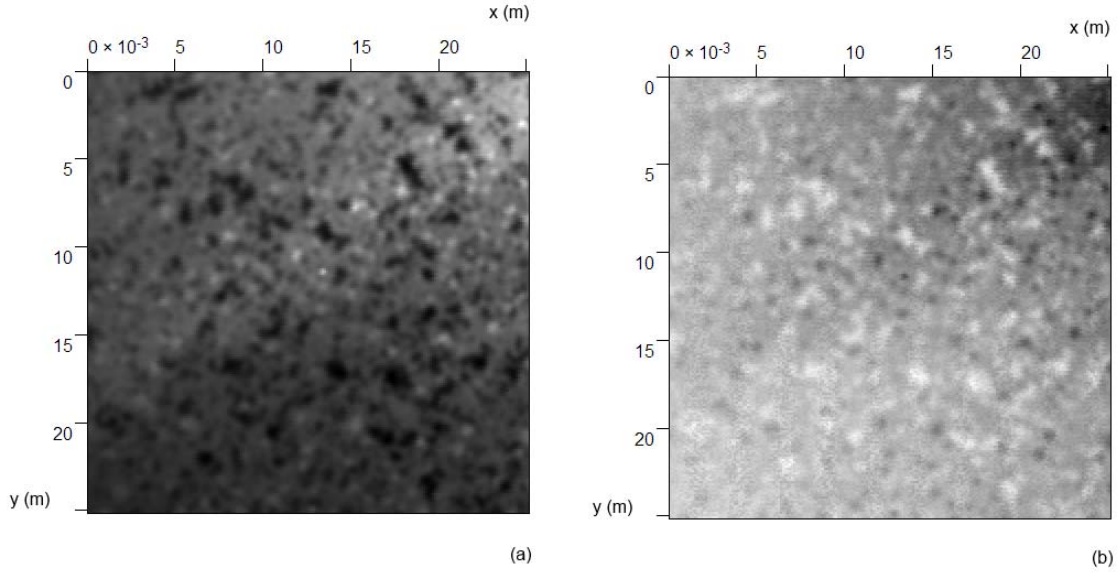

Figure 6. EPS surface scan of sandstone specimen; (a) output voltage data, (b) output phase data.

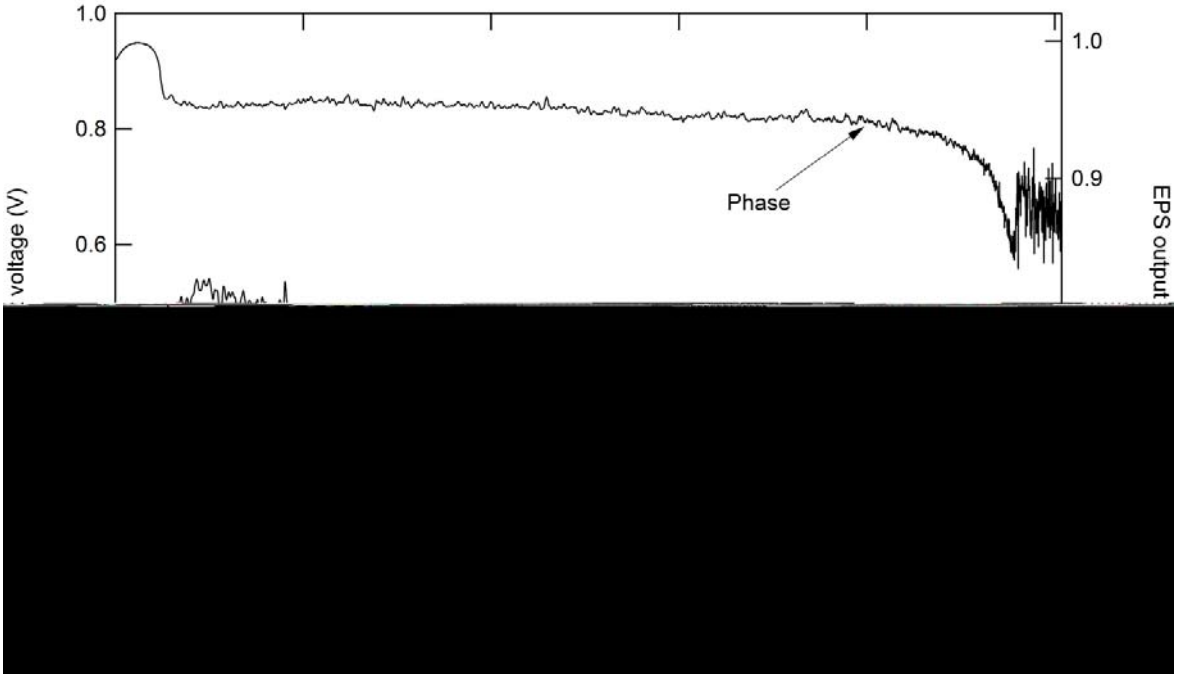

Figure 7. EPS line scan through length of sandstone specimen. Results show the EPS output voltage and phase.

Tables

Test Load\Current	0.1mA	0.5mA	1mA	10mA	20mA	30mA	50mA
10 Ω	0.0	0.0	0.0	7.0	9.0	9.0	10.0
	0.0	0.0	0.0	7.0	9.0	9.0	9.0
	0.0	0.0	0.0	7.0	9.0	9.0	10.0
100 Ω	0.0	53.0	81.0	98.0	100.0	100.0	102.0
	0.0	53.0	78.0	99.0	99.0	100.0	101.0
	0.0	53.0	78.0	98.0	99.0	99.0	101.0
1 kΩ	1381.0	1100.0	1021.0	1000.0	1000.0	1000.0	1000.0
	1381.0	1100.0	1021.0	1003.0	1004.0	1002.0	1002.0
	1381.0	1045.0	995.0	998.0	996.0	996.0	995.0
10 kΩ	16000.0	10300.0	10000.0	10000.0	10000.0	10000.0	10000.0
	15700.0	10620.0	9990.0	9990.0	9980.0	9980.0	9980.0
	16600.0	10280.0	10034.0	9813.0	9813.0	9813.0	9813.0
100 kΩ	150000.0	125000.0	125000.0	125000.0	125000.0	125000.0	125000.0
	145000.0	125000.0	125000.0	125000.0	125000.0	125000.0	125000.0
	148000.0	125000.0	125000.0	125000.0	125000.0	125000.0	125000.0

Table 1. Calibration data for Core Imaging system. All values expressed in Ohms, unless otherwise stated.